Metallic Adhesion Layer Induced Plasmon Damping and Molecular Linker as a Nondamping Alternative

Terefe G. Habteyes,[†,‡] Scott Dhuey,[§] Erin Wood,[§] Daniel Gargas,[§] Stefano Cabrini,[§] P. James Schuck,[§] A. Paul Alivisatos,[†,⊥] and Stephen R. Leone[†,‡,∥,*]

[†]Departments of Chemistry and [∥]Physics, University of California, Berkeley, California 94720, United States, and [‡]Chemical Sciences Division, [§]Molecular Foundry, and [⊥]Materials Sciences Division, Lawrence Berkeley National Laboratory, Berkeley, California 94720, United States

ABSTRACT

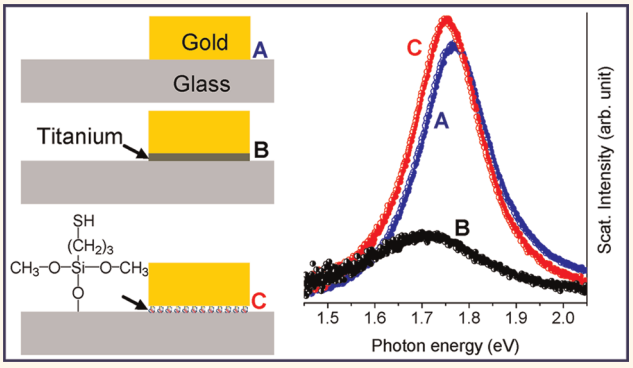

Drastic chemical interface plasmon damping is induced by the ultrathin (~2 nm) titanium (Ti) adhesion layer; alternatively, molecular adhesion is implemented for lithographic fabrication of plasmonic nanostructures without significant distortion of the plasmonic characteristics. As determined from the homogeneous linewidth of the resonance scattering spectrum of individual gold nanorods, an ultrathin Ti layer reduces the plasmon dephasing time significantly, and it reduces the plasmon scattering amplitude drastically. The increased damping rate and decreased plasmon amplitude are due to the dissipative dielectric function of Ti and the chemical interface plasmon damping where the conduction electrons are transferred across the metal—metal interface. In addition, a pronounced red shift due to the Ti adhesion layer, more than predicted using electromagnetic simulation, suggests the prevalence of interfacial reactions. By extending the experiment to conductively coupled ring-rod nanostructures, it is shown that a sharp Fano-like resonance feature is smeared out due to the Ti layer. Alternatively, vapor deposition of (3-mercaptopropyl)-trimethoxysilane on gently cleaned and activated lithographic patterns functionalizes the glass surface sufficiently to link the gold nanostructures to the surface by sulfur—gold chemical bonds without observable plasmon damping effects.

KEYWORDS: lithography · adhesion layer · chemical interface · plasmon damping · molecular adhesion

Collective oscillations of conduction band electrons known as localized surface plasmon resonances can be excited when metal nanostructures/nanoparticles interact with electromagnetic radiation in the appropriate frequency region. The collective oscillation decays due to various processes[1,2] such as radiation damping,[3] interband damping,[4,5] surface scattering,[6−8] and chemical interface damping,[8−10] leading to dephasing times (T_2) on the order of 10 fs. The importance of the different decaying mechanisms can depend on many factors such as the particle size and shape, the plasmon resonance energy, and the chemical environment. For example, the radiation damping, the loss due to conversion of the surface-bound wave (plasmon) into a photon, increases with the volume of the particle while the loss due to the surface scattering becomes important as the particle size decreases according to the proportionality $T_2 \propto R/v_F$, where v_F is the Fermi velocity and R is the particle radius.[1−3] When the resonance energy is within the interband electron transition edge, the plasmon decays rapidly due to electron−hole formation.[4] The dephasing time is a critical parameter for understanding the decay dynamics of the localized surface plasmon resonance. In addition, the dephasing time is directly related to the near-field amplitude, which is responsible for spectroscopic signal enhancement.[11] When the resonance spectra of individual nanostructures are measured, T_2 can be reliably determined from the homogeneous linewidth (Γ) using the relation $T_2 = h/(\pi\Gamma)$, where h is Planck's constant.[12] This approach has successfully been applied to understand the particle plasmon dephasing rate, and substantial differences have been observed in dephasing times based on the geometries of the particles.[4,11]

In lithographically fabricated noble metal nanostructures, the plasmon damping is exacerbated by the ultrathin adhesion layer that uses metals such as titanium (Ti) and chromium (Cr) due to chemical interface damping.[8−10] In the fabrication of integrated circuits,[13] Ti and other metallic adhesion

* Address correspondence to srl@berkeley.edu.

Received for review April 29, 2012 and accepted May 30, 2012.

Published online May 30, 2012
10.1021/nn301885u

layers are known to have a degrading effect due to interdiffusion[14] across the grain boundaries into the outer layer (*e.g.*, gold) and to subsequent oxidation reactions. As a result, other metals such as platinum and palladium are used as a diffusion barrier.[13,15] For plasmonic nanostructures, on the other hand, Ti (or Cr) is directly used as an adhesion layer for gold and silver nanostructures, and the effect of the underlying metal on the optical response has gained attention only recently.[16−19] For thin film plasmon sensors, it has been reported that a chromium adhesion layer decreases the sensitivity of reflectance change.[20] For gold split-ring resonators, it has been shown that the presence of a Ti layer leads to a resonance red shift and linewidth broadening.[18,19] However, the reports so far are based on ensemble measurements where the dephasing time cannot be extracted due to inhomogeneous broadening, and hence quantitative investigation of the Ti-induced interface plasmon damping is lacking. More importantly, to date, no alternative way of adhering the plasmonic nanostructures to the substrate has been presented.

In this work, first, the drastic plasmon damping effect of an ultrathin layer of Ti is quantified. By measuring the scattering spectra of individual nanostructures, the dephasing times are extracted from the homogeneous linewidth of the resonances. The plasmon decay dynamics of gold nanorods are discussed by comparing both the resonance energies and the dephasing times obtained in the absence or presence of an ultrathin Ti layer. The deviation of the observed results from predictions based on the bulk dielectric functions is attributed to interfacial reactions of Ti with the glass substrate and the gold layer. The roughness of the deposited materials surfaces is also expected to facilitate intermetallic diffusion through the grain boundaries, leading to the formation of Au−Ti compounds. The interpretations of the experimental results are supported with electromagnetic simulations that are carried out using the finite-difference time domain (FDTD) method.

We demonstrate a simple and efficient alternative for adhesion by using molecular linkers in the lithographic fabrication of gold nanostructures on a glass substrate. Specifically, it is shown that vapor deposition of (3-mercaptopropyl)trimethoxysilane (MPTMS) on as-developed e-beam-patterned glass/photoresist can effectively serve to covalently bind gold nanostructures on a glass substrate. It is well-known that the silane functional group [−Si(OCH$_3$)$_3$] of MPTMS reacts with the hydroxyl group of the glass surface forming Si−O−Si bonds, making the thiol group [−SH] available for S−Au bonding when gold is deposited on the top.[21,22] However, we note that the wet surface cleaning and activation (hydroxylation) procedures that are usually implemented in the formation of a self-assembled monolayer of MPTMS are not appropriate

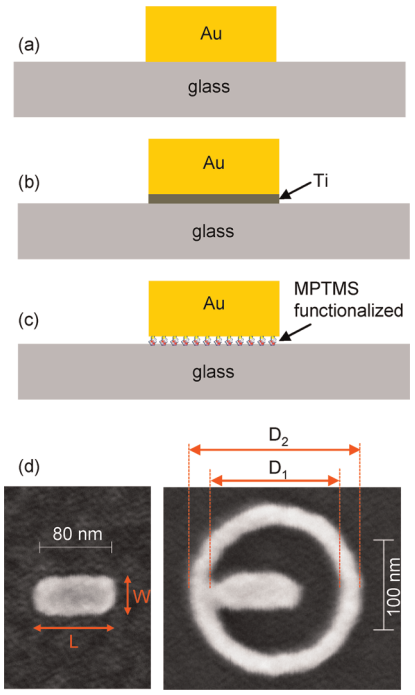

Figure 1. Schematics (a−c) showing how the gold nanostructures are supported on a glass substrate: (a) directly on glass, (b) on an ∼2 nm titanium adhesion layer, and (c) on MPTMS-functionalized surface. (d) Scanning electron microscope image of fabricated gold nanostructures with a thickness of ∼17 nm.

for the lithographic fabrication of nanostructures that involves liftoff procedures. The wet chemical treatment can easily dissolve the poly(methyl methacrylate) (PMMA) sacrificial layer that is used as a photoresist in the lithographic fabrication. It is also important to note that the MPTMS functionalization cannot be performed before the substrate is covered with the photoresist because the subsequent high-energy e-beam exposure can damage the molecular linker.[23] In this work, after the lithographic patterns are developed on the PMMA photoresist, the surface is gently activated applying ultraviolet/ozone (UVO) cleaning for a short period of time followed by vapor deposition of MPTMS. This procedure may not be expected to achieve uniform surface hydroxylation and MPTMS functionalization. However, arrays of gold nanostructures deposited on the pretreated glass substrate remain intact during the liftoff procedures even when vigorous sonication has been applied, indicating that the functionalization is sufficient to tether gold nanostructures to a glass substrate *via* sulfur−gold chemical bonding.

RESULTS AND DISCUSSION

The dephasing times and the resonance energies are investigated for three sets of arrays of gold nanostructures that are supported (a) directly on a glass, (b) on top of an ∼2 nm Ti adhesion layer, and (c) on MPTMS-functionalized glass, as shown in the schematics in

Figures 1a–c (see Methods section and Figure S1 of the Supporting Information for experimental details). We note that when the gold nanostructures are supported directly on a glass surface, a significant number of structures are washed away during the liftoff procedures. Representative scanning electron microscope (SEM) images of fabricated gold nanorod and ring-rod nanostructures are shown in Figure 1d. The average dimensions of the parameters are D_1 = 144 nm, D_2 = 190 nm, L = 85 nm, and W = 40 nm. The thickness of the gold nanostructures without the adhesion layer is ~17 nm. Scattering spectra for individual plasmonic nanostructures are acquired using a dark-field confocal microscope using excitation light that is polarized along the long axis of the nanorod.

Representative scattering spectra of the single nanorods are shown in Figure 2a, which can be compared with the calculated scattering cross section plotted in Figure 2b. The resonance peak is due to the longitudinal dipolar mode of the nanorod. Both the experimental and theoretical results show that the presence of the ~2 nm titanium adhesion layer significantly reduces the scattering intensity of the gold nanorod. The calculated absorption cross section shown in Figure 2c has an overall increased magnitude in the presence of Ti considering the total area under the broadened spectra. The near-field amplitude, which is directly proportional to the scattering cross section,[24] is significantly reduced in the presence of the Ti layer, as shown in Figure 2d. This drastic reduction of the plasmon amplitude is due to the dissipative imaginary part (ε_2) of the Ti dielectric function, $\varepsilon = \varepsilon_1 + i\varepsilon_2$. For example, at a photon energy of 1.7 eV, $\varepsilon = -3.98 + i16.4$ for titanium compared to $-18.7 + i1.2$ for gold. The near-field enhancement of a plasmonic material is proportional to the $|\varepsilon_1/\varepsilon_2|$ ratio[25] (see also Supporting Information Figure S2). The presence of the Ti deposit increases the rate of plasmon dephasing *via* charge transfer across the metal–metal interface, resulting in less confinement and greatly reduced near-field oscillation amplitude. The reduction of the near-field amplitude is consistent with the recent observation that the presence of a Ti or Cr adhesion layer results in reduced fluorescence signal enhancement.[17] It is known that for metal particles in metal matrices the particle plasmon can disappear due to chemical interface damping.[1,9] The result presented here demonstrates that the chemical interface damping effect is prevalent in the Au–Ti system even for ultrathin adhesion layers of Ti. While the values of the bulk dielectric constant used here may not be completely valid for simulating such small thicknesses of Ti, the results of the calculation in Figure 2b indicate that the damping effect is drastic even for 1 nm of Ti, compromising the use of Ti as an adhesion layer for plasmonic nanostructures, particularly in the visible region. The situation is worse for chromium as it is more absorptive than titanium.[16,26]

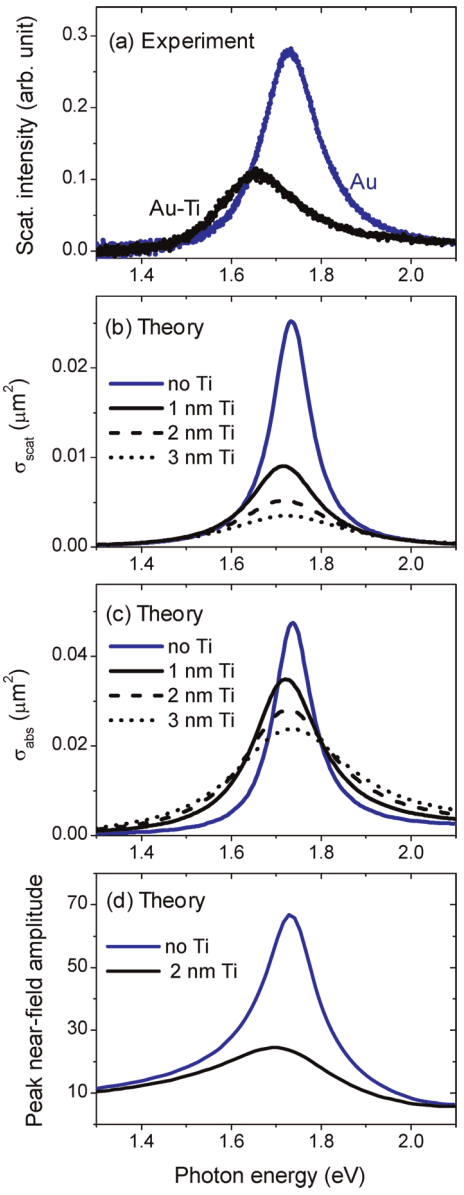

Figure 2. Measured and calculated spectra of gold nanorods. (a) Measured single particle scattering spectra for Au nanorod supported directly on a microscope cover glass (blue line) and on a ~2 nm Ti adhesion layer (black line), (b) calculated scattering cross section, (c) calculated absorption cross section, and (d) calculated near-field amplitude. The near-field amplitude is the peak (maximum) value in the *xz* plane that crosses the nanorod through its center longitudinally.

The plasmon resonance peak energy and the full width at half-maximum (linewidth, Γ) are determined by fitting Lorentzian functions to the measured scattering spectra. Although a polarizer is used to orient the electric field of the excitation light along the long axis of the nanorod, the spectra of some of the structures are slightly asymmetric due to the small contribution of the transverse (the short axis) mode, which peaks at ~0.45 eV higher than that of the longitudinal mode. Therefore, for reliable comparison, two Lorentzian functions are used throughout the fitting

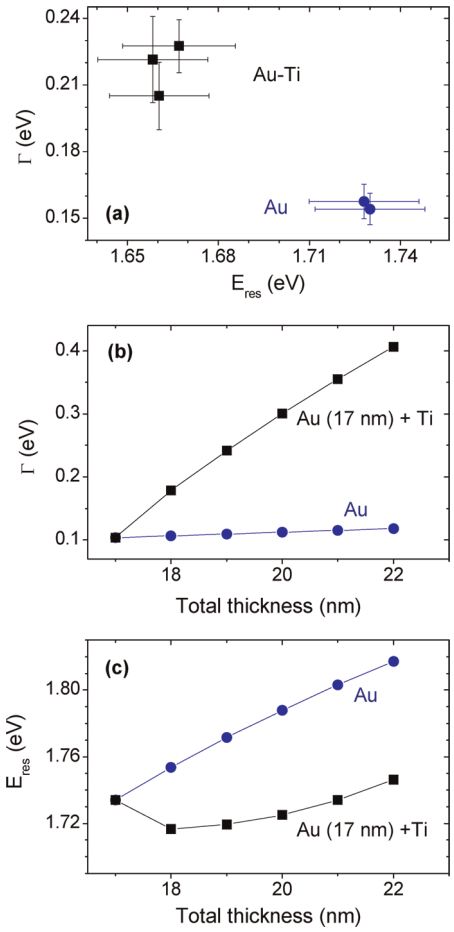

Figure 3. Experimental and calculated linewidths and resonance energies of gold nanorods. (a) Average linewidths as a function of resonance peak energy (E_{res}). Each data point represents the average linewidth and resonance energy extracted from the spectra of an array of 25 gold nanorods. Each set of nanostructures are obtained under slightly different electron doses of fabrication. (b) Linewidth extracted from the scattering spectra calculated for different total thickness of the nanorod. (c) Calculated resonance energy as a function of the nanorod total thickness.

procedure (see Figure S3), and only the parameters that are extracted from the longitudinal resonance peaks are considered in the discussion. The average parameters are summarized in Figure 3a; each data point, which represents slightly different electron doses during e-beam fabrication, is the average of parameters that are extracted from the spectra of about 25 nanorods.

Related to the plasmon damping, the spectral line width (Γ) is significantly broadened due to the Ti adhesion layer, as seen in the measured and calculated spectra in Figures 2a,b. When gold is supported directly on glass, $\Gamma = 156 \pm 7$ meV, which corresponds to $T_2 = 8.5 \pm 0.4$ fs. When the gold nanorods are deposited on top of ~2 nm Ti layers, the measured resonance linewidth is 216 ± 19 meV, a 40% increase compared to Au on glass. This Ti-induced linewidth broadening corresponds to a decrease of the dephasing time from 8.5 ± 0.4 fs to 6.1 ± 0.5 fs. In other words, the small fraction of Ti adhesion layer (~10% of the total thickness) results in an increase of the plasmon dephasing rate, T_2^{-1}, by ~40%. The average Γ plotted in Figure 3a has larger error bars for Au–Ti than for Au, which can be attributed to the uneven layer thickness of Ti for each nanostructure. For film thicknesses as thin as 2 nm of Ti, the electron beam evaporation process likely results in non-uniform (discontinuous) surface coverage, resulting in different values of plasmon damping for similar gold nanorods. The irregular film structure (see Figure S4) is difficult to exactly define in the simulation, and hence uniform thin films of Ti and gold are assumed in the calculation of the scattering cross sections. It is important, however, to note that the rough film structures of Ti and Au increase the plasmon dephasing rate through electron-surface scattering and radiation damping. The linewidths extracted from the calculated scattering spectra for Au and Au–Ti nanorods are plotted in Figure 3b. In qualitative agreement with the experimental result, the presence of a 2 nm Ti layer increases the linewidth from 104 to 242 meV. As the total thickness of the nanorod is increased by increasing the fraction of Ti, Γ increases rapidly (black line); when the thickness is increased by the same proportion, by increasing the fraction of Au, the change in Γ is insignificant (blue line).

When the gold nanorods are fabricated directly on a glass substrate, the resonance energy, on average, peaks at 1.729 ± 0.017 eV (717 ± 7 nm), which shifts to 1.661 ± 0.017 eV (747 ± 8 nm) when an ~2 nm Ti adhesion layer is used. The uncertainty indicates one standard deviation. According to the results of the calculation presented in Figure 3c, the resonance energy of the Au–Ti nanostructure is lower than that of pure gold, provided that the total thickness and other dimensions are the same. However, when the thickness of the Ti layer is increased while that of gold is fixed, the spectral peak energy first decreases and then increases continuously with increasing Ti thickness, which is due to the increased aspect ratio of the total thickness of the nanorod (Au + Ti) to its length. Comparing the spectra in Figures 2a,b, and considering the values plotted in Figures 3a,c, it can be seen that the experimental red shift is more pronounced than theoretically predicted. That is, the observed red shift (29 ± 8 nm) is reproducibly higher than the calculated shift (~6 nm). The results presented in Figure 3a confirm that the deviation cannot be due to slight structural differences of the fabricated Au–Ti and Au nanorods. Although variations in electron doses of fabrication produce slightly different sizes, the average resonance energies of the nanorods remain nearly the same as shown in Figure 3a.

The significant deviation of the calculated shift from the observed result can be explained by considering that a smooth interface boundary and bulk dielectric

functions of pure Au and Ti are assumed in the calculation. The granular surface structures of the deposited films are clearly seen in the atomic force microscope (AFM) and scanning electron microscope images (see Figure S4). As determined from the AFM images, the Au−Ti film deposited on a silicon wafer has root-mean-square deviation of 234 pm, compared to 75 pm for a silicon wafer, which is coated with a native oxide. However, as noted above, these structural defects that result from the metal deposition and also from the liftoff processes are not fully accounted for in the simulation. In addition, the simulation completely ignores any interfacial chemical reactions, which are known to be important. For example, in the experiment by Tisone and Drobek,[14] Ti−Au compounds such as Ti_3Au, TiAu, and $TiAu_2$ are detected in as-deposited films, suggesting that interdiffusion and subsequent reactions take place during the deposition. A diffusion coefficient (D) of $\sim 5 \times 10^{-15}$ cm^2/s was reported compared to 1×10^{-21} cm^2/s for bulk systems, indicating high defect density in the deposited films. This corresponds to a diffusion length $[2(tD)^{1/2}$, t is time] of ~10 nm per minute. In addition, titanium bonds to the glass substrate *via* oxide formation, the very characteristic for its use as an adhesion layer.[13] It is well-known that the plasmon resonance is sensitive to the refractive index of the surrounding medium.[27] Considering that oxides of titanium have characteristically high refractive indices (for example, a TiO_2 film[28] has a refractive index of 2.35 compared to ~1.5 for glass), even trace amounts of oxides at the interface can shift the resonance peak noticeably, resulting in a more pronounced red shift than theoretically predicted.

The combined effect of the linewidth broadening and resonance red shift is a reduced quality factor ($Q = E_{res}/\Gamma$), which is related to the field enhancement. Using the above values, it can be seen that Q is reduced from 11.1 to 7.7 due to the interface damping, which is a significant loss for nonlinear and surface-enhanced spectroscopic optical applications. For example, the Raman signal is proportional to Q^4, which means that the Ti-induced chemical interface damping reduces the signal enhancement by a factor of greater than 4.

One of the important applications of particle plasmon resonances is in monitoring slight changes in the refractive indices of chemical and biological media. These sensing applications require sharp resonance features. The adverse effect of the chemical interface plasmon damping on sharp resonance features is demonstrated by the optical response of conductively coupled ring-rod nanostructures (see SEM image in Figure 1c). As reported recently[29] and shown by the blue curve in Figure 4a, when the nanorod is linked to the nanoring by a neck-like conductive bridge, a quadrupole plasmon resonance of the ring is excited, peaking at ~1.38 eV. In addition, a Fano-like resonance is observed at 1.76 eV due to the destructive

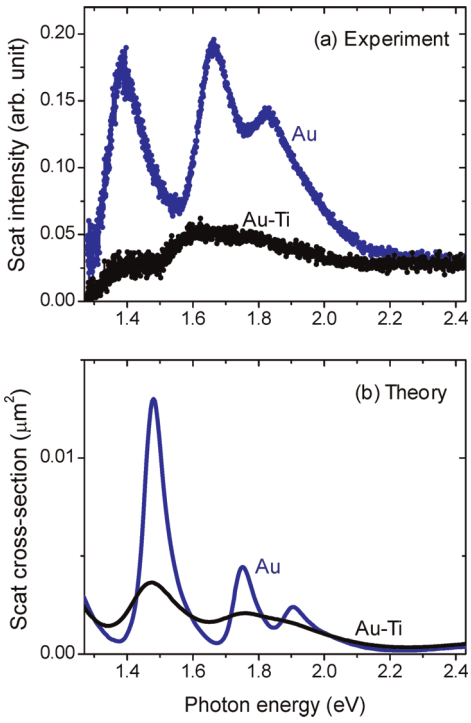

Figure 4. Scattering spectra of ring-rod gold nanostructure shown in Figure 1d. (a) Measured scattering spectra when the gold nanostructure is supported directly on a microscope cover glass (blue line) and on a ~2 nm Ti adhesion layer (black line). (b) Calculated scattering cross section.

interference of the octupolar resonance with the overlapping and broadened dipolar resonance. When similar ring-rod gold structures are supported on top of a 2 nm Ti adhesion layer, the overall scattering intensity is drastically reduced, and the Fano-like resonance feature is completely smeared out. This trend is reproduced in the calculated spectra, as seen in Figure 4b. The lower relative intensity of the quadrupolar resonance peak compared to the calculated one is due to the reduced efficiency of the detector close to the near-infrared region.

The discussion so far clearly underscores that using a metallic adhesion layer drastically reduces the plasmonic optical effect of noble metal nanostructures. Therefore, it is imperative that alternative adhesion mechanisms are sought. In the following, we discuss the implementation of readily available MPTMS as a molecular adhesion layer without compromising the optical effect of the plasmonic nanostructures.

A glass substrate is treated with MPTMS after the desired patterns are written on a PMMA sacrificial layer using e-beam lithography and development processes as described in the Methods section and in Figure S1, Supporting Information. In this procedure, the glass surface functionalization takes place only in the exposed areas defined by the e-beam lithography, as the remaining region is covered with the PMMA photoresist. A fused silica cover glass (Esco Products, Inc.) and a quartz wafer (Silicon Quest International, Inc.) have

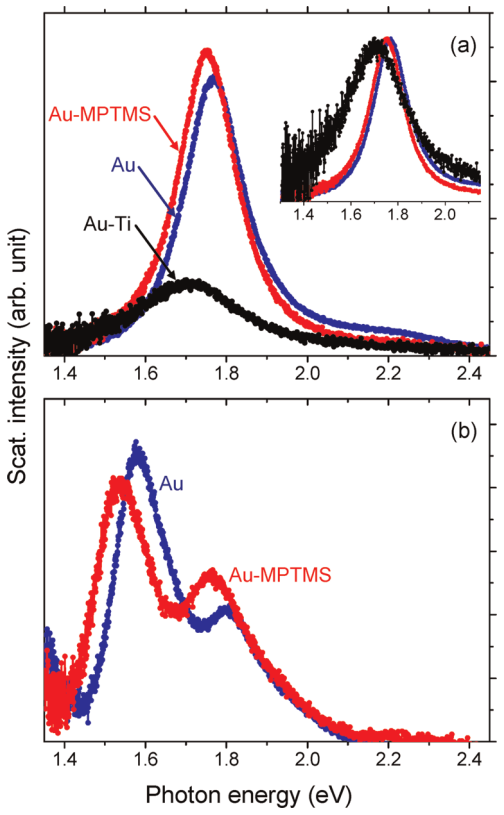

Figure 5. Scattering spectra of single gold nanorod (a) and ring-rod nanostructures (b) deposited directly on glass (blue line), on MPTMS-functionalized glass surface (red line), and on a ~2 nm Ti adhesion layer (black line). For the nanorod resonances in (a), the spectra normalized to the corresponding peaks are shown in the inset.

been used in this experiment, and the result is similar. In the case where the glass substrate is pretreated with MPTMS, nearly all of the structures remain at the desired location after the liftoff procedures. In the absence of the pretreatment, the yield varies dramatically; in some cases, nearly all of the structures are either washed away or distorted [compare (a) and (b) in Figure S5], and in other cases, the loss can be as low as 5% [compare (c) and (d) in Figure S5].

Representative scattering spectra of gold nanorods supported on three different regions (bare glass, ~2 nm Ti layer, and MPTMS-functionalized) of the same quartz wafer are compared in Figure 5a. Fabricating the nanostructures on the same wafer on top of different underlayers avoids the structural variations that result from different batches of fabrication, making the optical response comparison more reliable. In each case, more than 20 spectra of individual gold nanorods are evaluated. As shown in Figure 5a, the intensity and linewidth of the resonance scattering spectra of the gold nanorods that are deposited directly on glass and on MPTMS-pretreated surface are practically the same, considering the fluctuations even for nominally the same structures. As seen in Figure 5b, the sharp Fano-like resonance feature observed in a ring-rod structure is preserved when MPTMS is used as a molecular adhesion. In contrast for Au–Ti nanorods, the intensity is drastically reduced (black line in Figure 5a), and the linewidth is significantly broadened, resulting in smearing out of sharp resonance features.

CONCLUSION

Quantitative analyses of the chemical interface plasmon damping and resonance shifts are presented for Au–Ti nanorods in comparison with pure gold using single particle scattering spectroscopy. Using titanium as an example, it is demonstrated that a metallic embedding medium increases the plasmon dephasing rate, drastically reduces the plasmon amplitude, and red shifts the resonance peak. The increased dephasing rate is explained in terms of the dissipative dielectric function of the Ti and chemical interface damping where the conduction electrons are transferred across the metal–metal interface. The observed red shift is greater than predicted from electromagnetic simulation, which is based on the bulk dielectric functions of pure Au and Ti. The deviation is attributed to interface reactions and intermetallic diffusion processes, which are ignored by the calculation. By extending the experiment to conductively coupled ring-rod nanostructures, it is shown that sharp resonance features such as Fano-like resonances are smeared out completely due to the chemical interface plasmon damping, significantly reducing the usefulness of such features in sensing applications. It is shown that vapor deposition of (3-mercaptopropyl)trimethoxysilane on gently cleaned and activated lithographic patterns can efficiently link gold nanostructures to a glass substrate with no noticeable plasmon damping effect, and hence this fabrication method is proposed as a sound alternative for fabrication of plasmonic devices with improved performance. The molecular linker alternative presented here is based on the known S–Au covalent bond, and for other metals that do not form a strong chemical bond with sulfur, an ultrathin layer of gold can be used as an intermediary.

METHODS

Three types of arrays of gold nanostructures with 4 μm lattice spacing are fabricated using electron beam lithography and liftoff procedures: (1) directly on a glass, (2) on top of a ~2 nm titanium adhesion layer, and (3) on a MPTMS-functionalized glass surface, as shown in the schematics in Figure 1a–c. The fabrication process is summarized in Supporting Information, Figure S1. A cleaned glass substrate is spin-coated with 50 nm of poly(methyl methacrylate) (PMMA), a positive electron beam resist. To avoid charging effects during electron beam

exposure, a conductive polymer called aquaSAVE (Mitsubishi Rayon Co, Ltd.) is spin-coated on top of the PMMA. A defined area of the resist is exposed with an electron beam at 100 keV of energy, 500 pA of beam current, and ~2000 μC/cm^2 dose using a Vistec VB300 e-beam lithography system. After the aquaSAVE is removed by rinsing with water, the desired patterns are developed by dissolving the exposed part of the resist in a 7:3 ratio mixture (chilled to −5 °C) of isopropyl alcohol and water, applying sonication for 100 s. Films of Ti first and Au second are then deposited in vacuum (~10^{-7} Torr) all over the glass/PMMA surface using a Semicore SC600 evaporator, which focuses a ~10 keV e-beam on the materials contained in a crucible. Ti is deposited at a rate of ~1 Å/s to a final thickness of ~2 nm. Subsequently, Au is deposited at a rate of ~4 Å/s to a final thickness of ~17 nm. The PMMA and the metal film on top are removed *via* the liftoff procedure that involves immersing the sample in dichloromethane for ~15 min followed by immediate rinsing with isopropyl alcohol and sonication in acetone for 1−3 min.

For the Au glass and Au−Ti glass samples (discussed in Figures 2, 3, and 4), Au−Ti is directly deposited on the developed patterns. For the evaluation of MPTMS for molecular adhesion (Figure 5), the lithography, pretreatment, and evaporation processes are performed as follows. Three groups of structural features with the same structural parameters are developed in three regions on a quartz wafer of 100 mm diameter. In order to remove some residue of photoresist and activate the glass surface, UV-ozone cleaning is applied for 15 s (note that long time duration UV-ozone cleaning can affect the desired dimensions of the nanostructures). Gold is evaporated on region 1 while regions 2 and 3 are masked, and then Ti and Au are evaporated sequentially on region 2 while regions 1 and 3 are masked. The sample is then kept for 3 hours to 3 days in vacuum where there is an open vial filled with MPTMS. Gold is then evaporated on region 3 (MPTMS-functionalized glass surface), while regions 1 and 2 were masked. The PMMA photoresist is then removed by the liftoff procedures as described above. In all of our experiments, vapor deposition of MPTMS takes place at room temperature, and the adhesion performance appears to improve with longer deposition time. The reaction condition may further be improved by optimizing the deposition temperature.

The scattering spectra for individual nanostructures are acquired using a transmission mode dark-field confocal microscope (Nikon TE2000-U). The plasmonic resonances are excited with a white light (halogen lamp) that is polarized along the long axis of the nanorod and focused by an oil immersion dark-field condenser (numerical aperture, NA = 1.2−1.4) oriented normal to the sample surface. The light scattered by an individual nanostructure is collected with a 100×, 0.95 NA air objective. The scattered light is then directed through a 150 μm diameter pinhole and spectrally analyzed with a spectrometer (PI-Acton 2300i) equipped with a CCD camera that is cooled with liquid nitrogen. After the optical measurement is finalized, structural analysis is performed using a Zeiss Ultra 60 scanning electron microscope, avoiding the charging effect by coating the sample substrate with an ultrathin layer (less than 3 nm) of gold−palladium.

The electromagnetic simulations are performed using the finite-difference time domain (FDTD) method and implemented with Lumerical software. A total-field/scattered-field source scheme[30] is used to introduce light energy into the simulation region where the grid size is 1 nm in *x*, *y*, and *z* directions. The bulk dielectric constants of gold[31] and titanium[32] are used to model the nanostructures. The glass substrate is included in the calculation, and the calculated resonance peak energies match the observed ones when a background refractive index of 1.1 is used. For best estimates of the actual structures, the SEM images are directly imported into the simulation region and extruded along the *z*-direction to define the height. That is, except for the roughness of the surface, the simulation mimics the size and shape of the real (fabricated) nanostructures to the accuracy of the SEM.

Conflict of Interest: The authors declare no competing financial interest.

Acknowledgment. T.G.H. was supported by a University of California President's Postdoctoral Fellowship Program and recently on the NSF-EUV Engineering Research Center (No. EEC-0310717). Supplies and equipment are provided through the Materials Science Division (MSD), Lawrence Berkeley National Laboratory (LBNL), and the nanofabrication and optical measurements were performed as a user project at the Molecular Foundry, LBNL. The funds through the MSD and the work at the Molecular Foundry are supported by the Office of Science, Office of Basic Energy Sciences, of the U.S. Department of Energy under Contract No. DE-AC02-05CH11231.

Supporting Information Available: Schematics of the lithographic fabrication (Figure S1), field enhancement comparison for gold and titanium (Figure S2), analysis of plasmon resonance scattering spectra (Figure S3), visualization and analysis of Au−Ti surface roughness (Figure S4), and SEM images displaying the performance of MPTMS as an adhesion layer (Figure S5) are provided in the Supporting Information. This material is available free of charge *via* the Internet at http://pubs.acs.org.

REFERENCES AND NOTES

1. Kreibig, U.; Vollmer, M. *Optical Properties of Metal Clusters*; Springer: Berlin, 1995.
2. Hubenthal, F.; Hendrich, C.; Trager, F. Damping of the Localized Surface Plasmon Polariton Resonance of Gold Nanoparticles. *Appl. Phys. B: Lasers Opt.* **2010**, *100*, 225–230.
3. Wokaun, A.; Gordon, J. P.; Liao, P. F. Radiation Damping in Surface-Enhanced Raman Scattering. *Phys. Rev. Lett.* **1982**, *48*, 957.
4. Sonnichsen, C.; Franzl, T.; Wilk, T.; von Plessen, G.; Feldmann, J.; Wilson, O.; Mulvaney, P. Drastic Reduction of Plasmon Damping in Gold Nanorods. *Phys. Rev. Lett.* **2002**, *88*, 077402.
5. Pinchuk, A.; von Plessen, G.; Kreibig, U. Influence of Interband Electronic Transitions on the Optical Absorption in Metallic Nanoparticles. *J. Phys. D: Appl. Phys.* **2004**, *37*, 3133–3139.
6. Fuchs, K. The Conductivity of Thin Metallic Films According to the Electron Theory of Metals. *Proc. Cambridge Philos. Soc.* **1938**, *34*, 100–108.
7. Apell, P.; Monreal, R.; Flores, F. Effective Relaxation-Time in Small Spheres - Diffuse Surface Scattering. *Solid State Commun.* **1984**, *52*, 971–973.
8. Hovel, H.; Fritz, S.; Hilger, A.; Kreibig, U.; Vollmer, M. Width of Cluster Plasmon Resonances - Bulk Dielectric Functions and Chemical Interface Damping. *Phys. Rev. B* **1993**, *48*, 18178–18188.
9. Persson, B. N. J. Polarizability of Small Spherical Metal Particles - Influence of the Matrix Environment. *Surf. Sci.* **1993**, *281*, 153–162.
10. Kreibig, U. Interface-Induced Dephasing of Mie Plasmon Polaritons. *Appl. Phys. B: Lasers Opt.* **2008**, *93*, 79–89.
11. Klar, T.; Perner, M.; Grosse, S.; von Plessen, G.; Spirkl, W.; Feldmann, J. Surface-Plasmon Resonances in Single Metallic Nanoparticles. *Phys. Rev. Lett.* **1998**, *80*, 4249–4252.
12. Heilweil, E. J.; Hochstrasser, R. M. Nonlinear Spectroscopy and Picosecond Transient Grating Study of Colloidal Gold. *J. Chem. Phys.* **1985**, *82*, 4762–4770.
13. Lepselter, M. P. Beam-Lead Technology. *Bell Syst. Tech. J.* **1966**, *45*, 233.
14. Tisone, T. C.; Drobek, J. Diffusion in Thin-Film Ti−Au, Ti−Pd, and Ti−Pt Couples. *J. Vac. Sci. Technol.* **1972**, *9*, 271–275.
15. Pan, J. B.; Pafchek, R. M.; Judd, F. F.; Baxter, J. B. Effect of Chromium−Gold and Titanium−Titanium Nitride−Platinum−Gold Metallization on Wire/Ribbon Bondability. *IEEE Trans. Adv. Packag.* **2006**, *29*, 707–713.
16. Jiao, X. J.; Goeckeritz, J.; Blair, S.; Oldham, M. Localization of Near-Field Resonances in Bowtie Antennae: Influence of Adhesion Layers. *Plasmonics* **2009**, *4*, 37–50.
17. Aouani, H.; Wenger, J.; Gerard, D.; Rigneault, H.; Devaux, E.; Ebbesen, T. W.; Mahdavi, F.; Xu, T. J.; Blair, S. Crucial Role of

the Adhesion Layer on the Plasmonic Fluorescence Enhancement. *ACS Nano* **2009**, *3*, 2043–2048.
18. Lahiri, B.; Dylewicz, R.; De la Rue, R. M.; Johnson, N. P. Impact of Titanium Adhesion Layers on the Response of Arrays of Metallic Split-Ring Resonators (SRRs). *Opt. Express* **2010**, *18*, 11202–11208.
19. Jeppesen, C.; Mortensen, N. A.; Kristensen, A. The Effect of Ti and ITO Adhesion Layers on Gold Split-Ring Resonators. *Appl. Phys. Lett.* **2010**, *97*, 263103.
20. Ekgasit, S.; Thammacharoen, C.; Yu, F.; Knoll, W. Influence of the Metal Film Thickness on the Sensitivity of Surface Plasmon Resonance Biosensors. *Appl. Spectrosc.* **2005**, *59*, 661–667.
21. Goss, C. A.; Charych, D. H.; Majda, M. Application of (3-Mercaptopropyl)trimethoxysilane as a Molecular Adhesive in the Fabrication of Vapor-Deposited Gold Electrodes on Glass Substrates. *Anal. Chem.* **1991**, *63*, 85–88.
22. Mahapatro, A. K.; Scott, A.; Manning, A.; Janes, D. B. Gold Surface with Sub-nm Roughness Realized by Evaporation on a Molecular Adhesion Monolayer. *Appl. Phys. Lett.* **2006**, *88*, 151917.
23. Seshadri, K.; Froyd, K.; Parikh, A. N.; Allara, D. L.; Lercel, M. J.; Craighead, H. G. Electron-Beam-Induced Damage in Self-Assembled Monolayers. *J. Phys. Chem.* **1996**, *100*, 15900–15909.
24. Messinger, B. J.; Vonraben, K. U.; Chang, R. K.; Barber, P. W. Local-Fields at the Surface of Noble-Metal Microspheres. *Phys. Rev. B* **1981**, *24*, 649–657.
25. Sarid, D.; Challener, W. *Modern Introduction to Surface Plasmons*; University Press: Cambridge, UK, 2010.
26. Sexton, B. A.; Feltis, B. N.; Davis, T. J. Characterisation of Gold Surface Plasmon Resonance Sensor Substrates. *Sens. Actuators, A* **2008**, *141*, 471–475.
27. Liedberg, B.; Nylander, C.; Lundstrom, I. Surface-Plasmon Resonance for Gas-Detection and Biosensing. *Sens. Actuators* **1983**, *4*, 299–304.
28. Lehmann, H. W.; Frick, K. Optimizing Deposition Parameters of Electron-Beam Evaporated TiO_2 Films. *Appl. Opt.* **1988**, *27*, 4920–4924.
29. Habteyes, T. G.; Dhuey, S.; Cabrini, S.; Schuck, P. J.; Leone, S. R. Theta-Shaped Plasmonic Nanostructures: Bringing ″Dark″ Multipole Plasmon Resonances into Action *via* Conductive Coupling. *Nano Lett.* **2011**, *11*, 1819–1825.
30. Taflove, A.; Hagness, S. C. *Computational Electrodynamics The Finite-Difference Time-Domain Method*; Artech House: Boston, MA, 2005.
31. Johnson, P. B.; Christy, R. W. Optical-Constants of Noble-Metals. *Phys. Rev. B* **1972**, *6*, 4370–4379.
32. Palik, E. D. *Handbook of Optical Constants of Solid*; Elsevier: Amsterdam, 1998.